Materials Characterization 181 (2021) 111502

Contents lists available at ScienceDirect

Materials Characterization

journal homepage: www.elsevier.com/locate/matchar

Effect of Y addition on microstructure evolution and precipitation of Cu-Co-Si alloy during hot deformation

Pengfei Yang [a,b,c], Meng Zhou [a,b,c,*], Yi Zhang [a,b,c,*], Yanlin Jia [d], Baohong Tian [a,b,c], Yong Liu [a,b,c], Xu Li [e], Alex A. Volinsky [f]

[a] School of Materials Science and Engineering, Henan University of Science and Technology, Luoyang 471023, PR China
[b] Provincial and Ministerial Co-construction of Collaborative Innovation Center for Non-ferrous Metal New Materials and Advanced Processing Technology, Luoyang 471023, PR China
[c] Henan Key Laboratory of Nonferrous Materials Science and Processing Technology, Luoyang 471023, PR China
[d] School of Materials Science and Engineering, Central South University, Changsha 410083, PR China
[e] Center for Advanced Measurement Science, National Institute of Metrology, Beijing 100029, PR China
[f] Department of Mechanical Engineering, University of South Florida, 4202 E. Fowler Ave. ENG030, Tampa 33620, USA

ARTICLE INFO

Keywords:
Cu-Co-Si and Cu-Co-Si-Y alloys
Hot deformation
Constitutive equations
Microstructure evolution
Precipitates

ABSTRACT

The effects of Y for the microstructure evolutions of Cu-Co-Si alloys during hot deformation were investigated. The hot deformation behaviors for Cu-2.6Co-0.65Si and Cu-2.6Co-0.65Si-0.2Y alloys were carried out on the Gleeble-1500 simulator with the strain rates from 0.001 to 10 s^{-1} and temperatures from 500 °C to 900 °C. The hot deformation activation energies for two copper alloys were calculated and the constitutive equations were also established. According to the true stress-strain curves and EBSD image analysis, it showed that the nucleation of dynamic recrystallization (DRX) grain and the growth of DRX grain were promoted with the addition of 0.2 wt% Y. Electron backscatter diffraction (EBSD) was used to characterize the microstructure of the hot deformed Cu-Co-Si alloy. The electrode diagram and ODF diagram were established to analyze the textures. The texture strength and the number of small angle grain boundaries were reduced by the addition of 0.2 wt% Y. The microstructure of two alloys was analyzed by transmission electron microscopy, it was found that a large number of Co_2Si nanoparticles were distributed on the copper matrix. Y could promote the precipitation process of δ-Co_2Si, and these nanoparticles interacted with dislocations during the hot deformation process to improve the deformation resistance.

1. Introduction

Copper alloys are widely used in lead frames and electronic connectors due to their excellent conductive, thermal properties and good corrosion resistance [1–5]. With the development of electronic products towards to thinness and intelligence, the copper alloys are required to have more different performances, which mean the more different kinds of copper alloy are needed. For example, the energy consumption of integrated circuits is multiplying with the continuous increasing of the scale, which not only requires good heat dissipation ability, but also needs excellent electrical conductivity and enough mechanical strength for the lead frame copper alloy.

In recent years, Cu-Ni-Co-Si alloys has been the focused by many researchers, because the Co and Ni can be a good partner, and the δ-(Co, Ni)$_2$Si precipitates formed by combining with Si can greatly improve the properties of copper matrix. Generally, the study added different contents of Co into Cu-Ni-Si alloy, and explored the effect of Co on the microstructure and properties of Cu-Ni-Si alloy. Huang et al. [6] used two thermo-mechanical treatment on Cu-4.5Ni-1.2Co-1.0Si-0.15 Mg, and found that the addition of Co can promoted the precipitation of nanometer δ-(Co,Ni)$_2$Si particles and improved the comprehensive properties of the alloy. However, from the investigations of Zhao et al. [7] found that the increase of Co content had a negative effect on the properties of Cu-1.5Ni-1Co-0.6Si alloy with accelerating the aging process and the growth of precipitates. Xiao et al. [8] also obtained a similar conclusion. Therefore, the amount of Co must be kept in a reasonable range. Li et al. [9] designed new Cu-Ni-Co-Si alloys which had different Ni/Co mass ratios under the premise of ensuring (Ni + Co) /Si mass ratio

* Corresponding authors at: School of Materials Science and Engineering, Henan University of Science and Technology, Luoyang 471023, PR China.
E-mail addresses: zhoumeng0902@126.com (M. Zhou), yizhang@haust.edu.cn (Y. Zhang), jiayanlin@126.com (Y. Jia).

https://doi.org/10.1016/j.matchar.2021.111502
Received 26 July 2021; Received in revised form 9 September 2021; Accepted 30 September 2021
Available online 4 October 2021

of 4.2, and found that the Ni/Co ratio was 1.95, the volume fraction and density of precipitated phase were the highest, resulting in the highest microhardness.

Since Co is more difficult to be solidly dissolved into copper matrix than Ni, it is necessary to explore some new alloying elements which can promote the solid solution and precipitation of Co in copper matrix, and relevant studies have been carried out. It is a common method to study the effect of alloying elements on microstructure and precipitated phase of Cu-Ni-Co-Si alloy during thermal deformation. In our previous studies on deformation, Ban et al. [10] investigated the effect of addition Cr on the constitutive equation and precipitates of Cu-Ni-Co-Si alloy, and confirmed that the addition of alloying element Cr refined the recrystallized grains and precipitates through the analysis of the microstructure. Geng et al. [11,12] investigated the effects of addition Ti and rare Ce on the microstructure evolution and precipitation of Cu-Co-Si-Ti alloy during hot deformation, and confirmed that the addition of Ti and Ce also refined the precipitated phase and promoted dynamic recrystallization.

Based on the above researches, Cu-2.6Co-0.65Si alloy Cu-2.6Co-0.65Si-0.2Y alloys were prepared by adding 0.2 wt% rare earth element Y and excluding the influence of Ni element. The Gleeble thermal simulator was used to study the hot compression process at strain rates of 0.001–10 s^{-1} and deformation temperatures of 500–900 °C. This method was commonly used in the study of various non-ferrous metals, iron and steel materials, such as Al [13,14], Cu [15], Mg [16], Ni [17], Ti [18] and Fe [19]. The JSM-7800F backscatter scanning electron microscopy and JEM-2100 transmission electron microscopy were used to analyze the hot deformation samples. The flow stress, hot deformation activation energy and EBSD data were obtained and compared. Effect of Y addition on microstructure evolution and precipitation of Cu-Co-Si alloy during hot deformation were analyzed.

2. Experimental materials and procedures

The amount and type of rare earth elements may affect the microstructure and precipitates of the alloy. After the study of relevant researches [12,20–24], 0.2 wt% Y was added into the Cu-Co-Si alloy. Considering the burning loss of Y in the melting process, Cu-7%Y master alloy was selected as the intermediate total and the addition amount of Y was increased. Cu-2.6Co-0.65Si and Cu-2.6Co-0.65Si-0.2Y alloys were prepared by using standard electrolytic copper, pure cobalt, pure nickel and Cu-7%Y master alloy as raw materials which were melted by ZG-0.01-40-4 vacuum intermediate frequency induction furnace. In the melting process, pure cobalt, pure silicon and Cu-7%Y master alloy were put into the graphite crucible for smelting in turn by the first large amount and then small amount, also first high melting point and then low melting point. The molten alloy was poured into a sand mold with a diameter of 90 mm and covered with a little charcoal.

After ingots were cooled to room temperature, the riser and surface oxide scale were removed. Due to the high thermal expansion coefficients of copper alloys, a large number of shrinkage porosity, shrinkage cavity and thermal stress were produced in the ingots during cooling, so it was necessary to carry out hot extrusion. The ingots were heated to 1030 °C in a box-type resistance furnace and held for 2 h to eliminate internal stress, and then extruded in the XJ-500 metal profile extruder. The head and tail of the extruded bar were cut off, and the segments were treated with solid solution. The heating rate was 10 °C·s^{-1} for 95 min and the temperature was heated to 950 °C for 90 min. After solution, the round bar was cut into cylindrical samples with a diameter of 8 × 12 mm for the hot compression test. The strain temperatures of 700 °C, 750 °C, 800 °C°C, 850 °C, 900 °C and strain rates of 0.001 s^{-1}, 0.01 s^{-1}, 0.1 s^{-1}, 1 s^{-1}, and 10 s^{-1} were selected for the hot deformation on Gleeble-1500D thermal simulated test machine.

The JSM-7800F backscatter scanning electron microscopy (SEM) and JEM-2100 transmission electron microscopy (TEM) were used to observe the microstructure evolution of the two alloys at different temperatures and strain rates. The 1 mm thick sheets were prepared from the middle of the samples. After the specimens were inserted, ground, mechanically polished and electropolished, the electron backscatter diffraction (EBSD) for the alloy was observed by JSM-7800F backscatter scanning electron microscope. The thin sections were thinned to 0.1 mm with metallographic sandpaper, and then treated with ion thinning. The microstructure of the precipitates was observed by JEM-2100 transmission electron microscope.

3. Results and discussion

3.1. True stress-true strain curves

The stress-strain curves of Cu-2.6Co-0.65Si and Cu-2.6Co-0.65Si-0.2Y alloys at different strain rates and deformation temperatures are shown in Fig. 1. In the process of hot deformation, the stress value of the alloy was usually affected by work hardening, dynamic recovery and dynamic recrystallization [12]. The variation of the curves can be divided into three stages. In the first stage, the stress increased rapidly with the strain, mainly affected by work hardening. In the second stage, the influence of dynamic recovery and recrystallization was gradually equivalent to work hardening. The growth rate of flow stress slowed down gradually, and the curve was in a horizontal state, reached the maximum value and remained stable. In the third stage, the effect of dynamic recovery and dynamic recrystallization was more obvious, and showed a downward trend.

Fig. 1 shows the True stress-strain curves of Cu-2.6Co-0.65Si and Cu-2.6Co-0.65Si-0.2Y alloy at different temperatures and strain rates. Take the Cu-2.6Co-0.65Si alloys deformed at the strain rate of 0.001 s^{-1} as an example, the temperature increased from 500 °C to 900 °C, the peak stress of the alloy was reduced from 267.9 to 68.8 MPa due to the temperatures increased and the average kinetic energy of atoms were promoted and the dynamic recovery and recrystallization were improved [25]. In addition, the flow stress increased with the increased of strain rates, such as Cu-2.6Co-0.65Si deformed at the temperature of 600 °C with the strain rates changed from 0.001 to 10 s^{-1}, and the peak stress increased from 251 to 309.6 MPa. Under the condition of high strain rates, the increased of strain rates for the DRX provided more drive energy. One hand, it greatly promoted the DRX into the nucleation process. Other hand, the fine DRX grains grew up too late and relatively obtained with much more high flow stress [15].

Compared the true stress-strain curves of Cu-2.6Co-0.65Si and Cu-2.6Co-0.65Si-0.2Y, it can be seen that the flow stress of Cu-2.6Co-0.65Si-0.2Y alloy was generally higher than Cu-2.6Co-0.65Si alloy at 500 °C. It is proved that the addition of Y can increase the flow stress of Cu-Co-Si alloy, and increase the deformation resistance in the process of hot deformation.

3.2. Hot deformation activation energy and constitutive equation

The flow stress is often controlled by strain rates ($\dot{\varepsilon}$) and deformation temperatures (T), and this is also a behavior of thermal activation [26]. The occurrence of such behavior requires the atoms to reach a certain kinetic energy, which was called hot deformation activation energy. According to push the thermal deformation to activate the constitutive equation, the relationships between the rheological stress(σ), strain rate ($\dot{\varepsilon}$) and deformation temperature (T) were deduced at the same time. By taking Cu-2.6Co-0.65Si-0.2Y alloy as an example, the constitutive equation was established in details according to introduce the hyperbolic sine model. The expression of hyperbolic sine model proposed by Sellars [27] and Mctegart [28] et al. is as follows:

$$\dot{\varepsilon} = A\left[sinh(\alpha\sigma)^{n} exp\left(-\frac{Q}{RT}\right)\right] \quad (1)$$

In the epsilon-strain rate, s^{-1}; σ-stress, MPa; Q- thermal activation

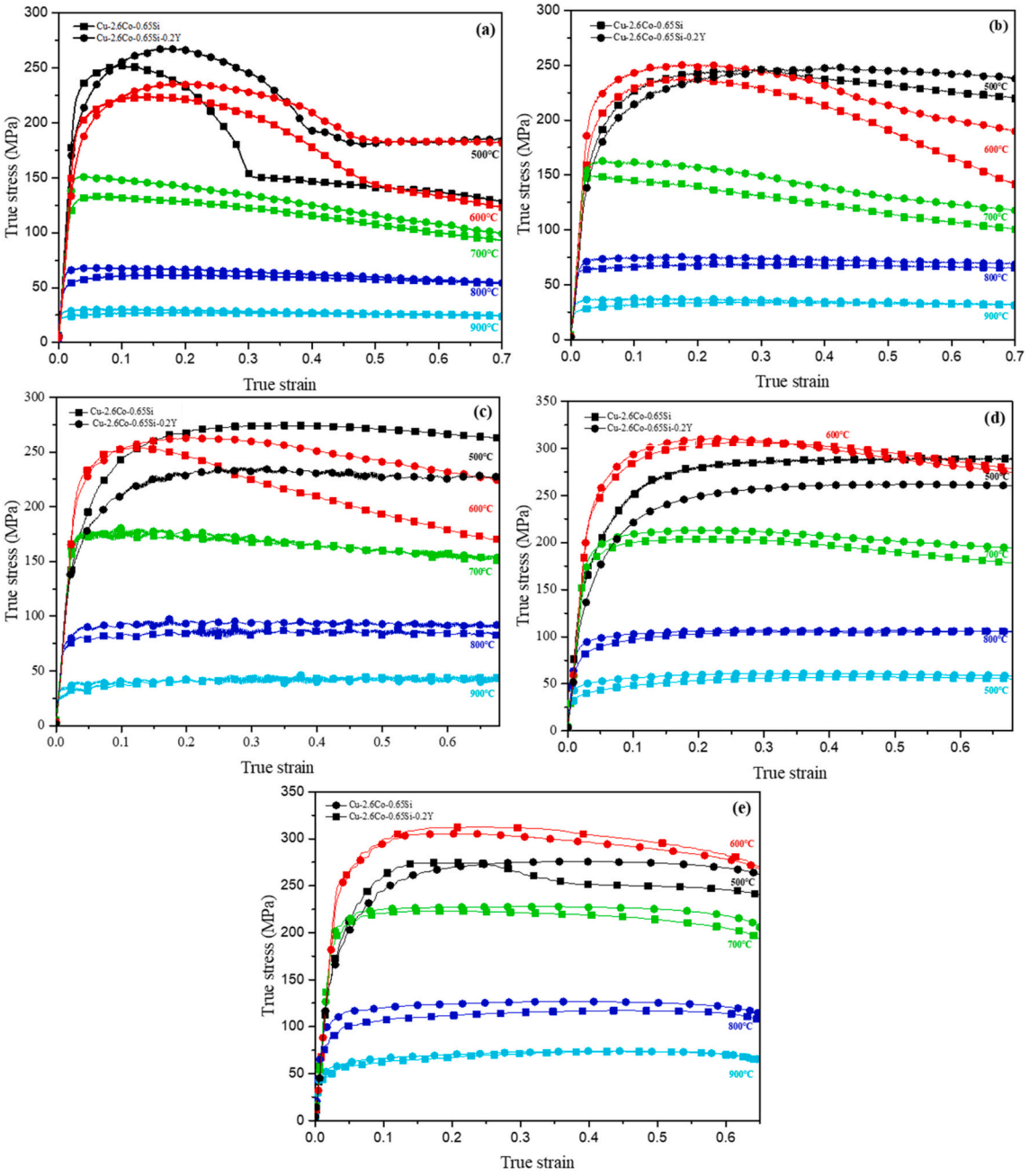

Fig. 1. True stress-True strain curves of Cu-2.6Co-0.65Si and Cu-2.6Co-0.65Si-0.2Y alloys at strain rates of: (a) 0.001 s^{-1}, (b) 0.01 s^{-1}, (c) 0.1 s^{-1}, (d) 1 s^{-1}, (d) 10 s^{-1}.

energy, $J{\cdot}mol^{-1}$; R- gas constant, 8.314 $J{\cdot}mol^{-1}{\cdot}\,k^{-1}$; T- temperature, K; A, n are all constants.

Eq. (1) is the function of stress, which can be subdivided into the following two different forms at different strains under different conditions:

$$\dot{\varepsilon} = A_1\sigma^{n_1} exp\left(-\frac{Q}{RT}\right) \ (\alpha\sigma < 0.8) \tag{2}$$

$$\dot{\varepsilon} = A_2 exp(\beta\sigma) exp\left[-\frac{Q}{RT}\right] \ (\alpha\sigma > 1.2) \tag{3}$$

The parameter Z is used to represent the lattice self-diffusion energy due to dislocation slip and climb:

$$Z = \dot{\varepsilon} exp\left[\frac{\dot{Q}}{RT}\right] \tag{4}$$

Substituting Eq. (4) into Eq. (1), we can get:

$$Z = [sinh(\alpha\sigma)]^n \tag{5}$$

Logs of both sides of Eqs. (2), (3) and (5) are obtained:

$$ln\dot{\varepsilon} = n_1 ln\sigma + lnA_1 - \frac{Q}{RT} \tag{6}$$

$$ln\dot{\varepsilon} = \beta\sigma + lnA_1 - \frac{Q}{RT} \tag{7}$$

$$lnZ = lnA + nln[sinh(\alpha\sigma)] \tag{8}$$

Assuming the temperature T and strain rate remain the same, the partial derivative of both sides of Eqs. (1) with respect to $1/T$ should give the hot deformation activation energy to be expressed as follows:

$$Q = R\left[\frac{\partial(ln\dot{\varepsilon})}{\partial ln[sinh(\alpha\sigma)]}\right]_T\left[\frac{\partial ln[sinh(\alpha\sigma)]}{\partial(1/T)}\right] = Rn_1S \tag{9}$$

β is the draw value of the slope in Fig. 2 (a), and β is calculated as 0.123656; n_1 is the draw value of the slope in Fig. 2 (b), and n_1 is calculated as 19.1265, $\alpha = \beta/n_1 = 0.00646$; n is the draw value of the slope in Fig. 2 (c), and n is calculated as 12.54582; S is the draw value of the slope in Fig. 2 (d), and S is calculated as 5.11589; The intercept of Fig. 2 (e) is ln A, ln $A = 63.646$, $A = e^{63.646}$.

Hot deformation activation energy can be calculated:

$$Q = RnS = 8.314 \times 12.54582 \times 5.11589 = 533.618\ \text{kJ·mol}^{-1}$$

Constitutive equation of Cu-2.6Co-0.65Si-0.2Y alloy can be expressed as follow:

$$\dot{\varepsilon} = e^{63.646}[sinh(0.00646\sigma)]^{12.546}exp\left(-\frac{533.618}{8.314T}\right) \tag{10}$$

Similarly, the activation energy of hot deformation and the constitutive equation of Cu-2.6Co-0.65Si alloy can be obtained.

Hot deformation activation energy can be calculated:

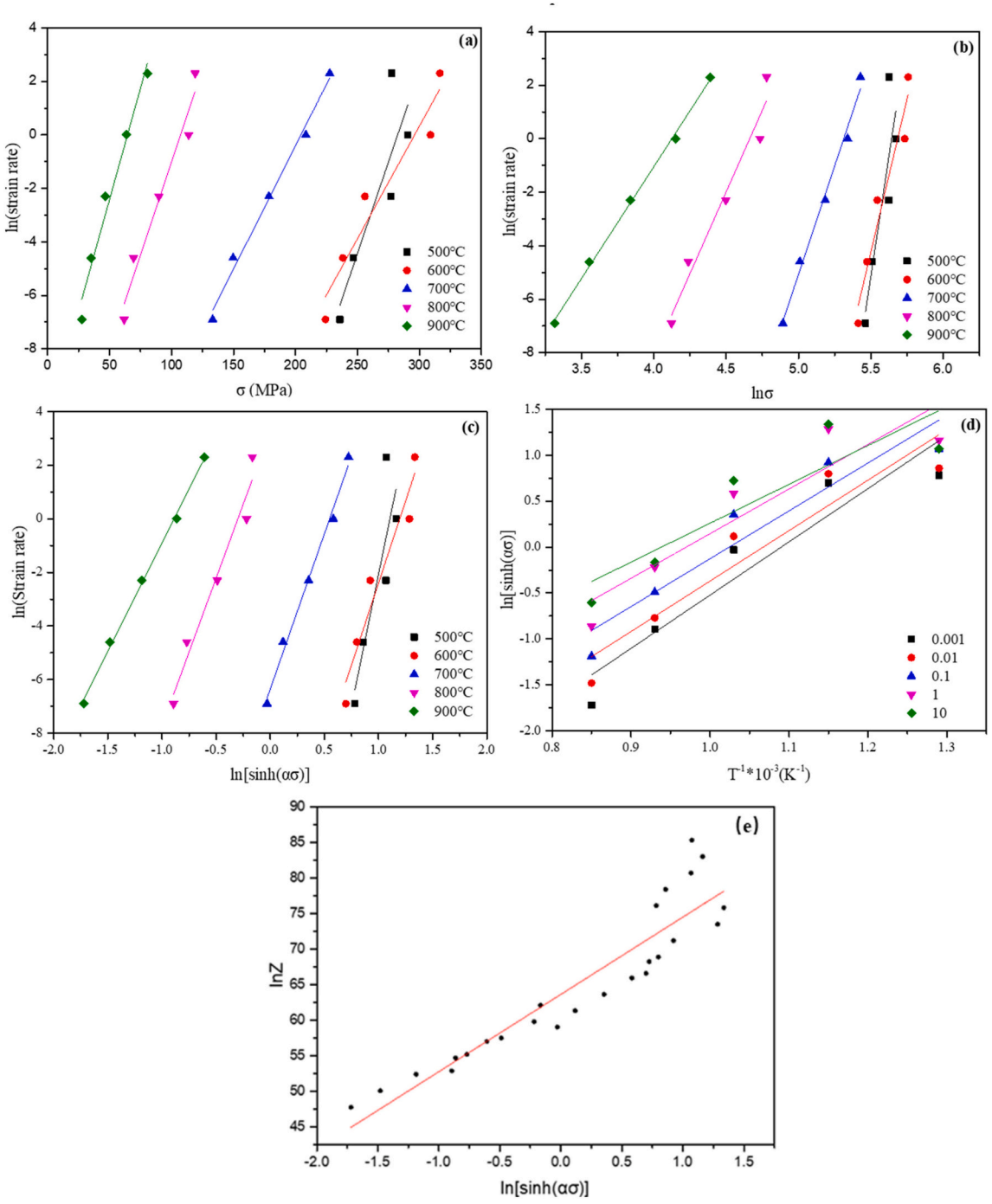

Fig. 2. Relationships between: (a) ln (strain rate) and σ; (b) ln (strain rate) and ln σ; (c) ln (strain rate) and ln [sinh ($\alpha\sigma$)]; (d) ln [sinh ($\alpha\sigma$)] and $T^{-1}(10^{-3}K)^{-1}$; (e) ln Z and ln [sinh ($\alpha\sigma$)].

$$Q = RnS = 8.314 \times 11.91453 \times 4.99171 = 494.466\ \text{kJ·mol}^{-1}$$

Constitutive equation of Cu-2.6Co-0.65Si alloy can be expressed as:

$$\dot{\varepsilon} = e^{57.943}[sinh(0.00664\sigma)]^{11.914} exp\left(-\frac{494.466}{8.314T}\right) \quad (11)$$

In contrast, by the addition of 0.2 wt% Y can increase the hot deformation activation energy of Cu-2.6Co-0.65Si alloy. Rare earth elements promoted the precipitation of solute atoms to purify the copper matrix, which can make the microstructure more uniform and the hot deformation more difficult, and the hot deformation activation energy was improved [25,29].

3.3. EBSD analysis

The original EBSD data for Cu-2.6Co-0.65Si and Cu-2.6Co-0.65Si-0.2Y were obtained by JSM-7800F backscatter electron microscopy which can be used to analyze the texture, grain size and orientation error of the alloy after hot deformation [30,31]. Fig. 3 shows EBSD images of Cu-2.6Co-0.65Si-0.2Y and Cu-2.6Co-0.65Si alloys under different conditions.

Fig. 3(a) and (c) are EBSD images of Cu-2.6Co-0.65Si and Cu-2.6Co-0.65Si-0.2Y alloys at 700 °C, respectively. There are many fine recrystallized grains around the coarse deformed grains, which was called a typical "necklace" structure [32]. Moreover, the number of recrystallized grains in Fig. 3 (a) is much more than Fig. 3 (c), which was indicated that REE Y plays a significant role in promoting the nucleation of DRX grains in Cu-2.6Co-0.65Si alloy. Whether CDRX or DDRX, one of the conditions for DRX can provide the energy needed for nucleation. According to the above conclusions, under the same hot deformation condition, the flow stress of Cu-2.6Co-0.65Si-0.2Y alloy is larger, which means that the alloy stores more energy required by DRX.

Fig. 3 (c) and Fig. 3 (d) are EBSD images of Cu-2.6Co-0.65Si-0.2Y alloy at 700 °C and 900 °C, respectively. When the temperature increased from 700 °C to 900 °C, the DRX grains gradually grew up and consumed the coarse deformed grains and other fine DRX grains. Under the higher temperature, DRX grains with higher proportion and larger size can be obtained, which was in line called the typical DRX behavior in metals [32,33]. This is because the temperature increased the average kinetic energy of the atoms, which in turn promoted the migration of DRX grain boundaries and the growth of grains. There are a few twins in Fig. 3 (d), which is due to the increase of temperature which promotes the formation of twins [33].

Fig. 4 shows the EBSD orientation maps of Cu-2.6Co-0.65Si and Cu-2.6Co-0.65Si-0.2Y alloys at 0.01 s^{-1} and different temperatures, in which the low-angle boundary ($5° < \theta < 10°$) and large high-angle boundary ($\theta < 15°$) were represented by a thin yellow-green line and a thick black line. It can be seen from the figures that the distribution of misorientation angle was basically the same, and there was a considerable concentration at the low misorientation angle, which was related to the amount of stored dislocation. In the process of dynamic recrystallization, the rotation of subgrain boundaries caused small sub-grains to merge into large subgrains, and the orientation errors between large subgrains and adjacent subgrains increased, forming large angle grain boundaries [34]. High temperatures will promote the migration of large-angle grain boundaries, phagocyte the dislocations along the path, thereby reducing the number of small-angle grain boundaries and forming equiaxed grains with only a few dislocations [35].

Cu-2.6Co-0.65Si and Cu-2.6Co-0.65Si-0.2Y can produce a lot of dislocations during hot deformation. The agglomeration of dislocations within grain boundaries can form small-angle grain boundaries, which can provide energy for nucleation of DRX, and the increase of temperatures will further promote the growth of DRX grains until the deformed grains are engulfed. For example, Fig. 4 (a) and (c) show the orientation of Cu-2.6Co-0.65Si and Cu-2.6Co-0.65Si-0.2Y alloys deformed at 700 °C respectively. Rare earth elements promote the nucleation of DRX grains

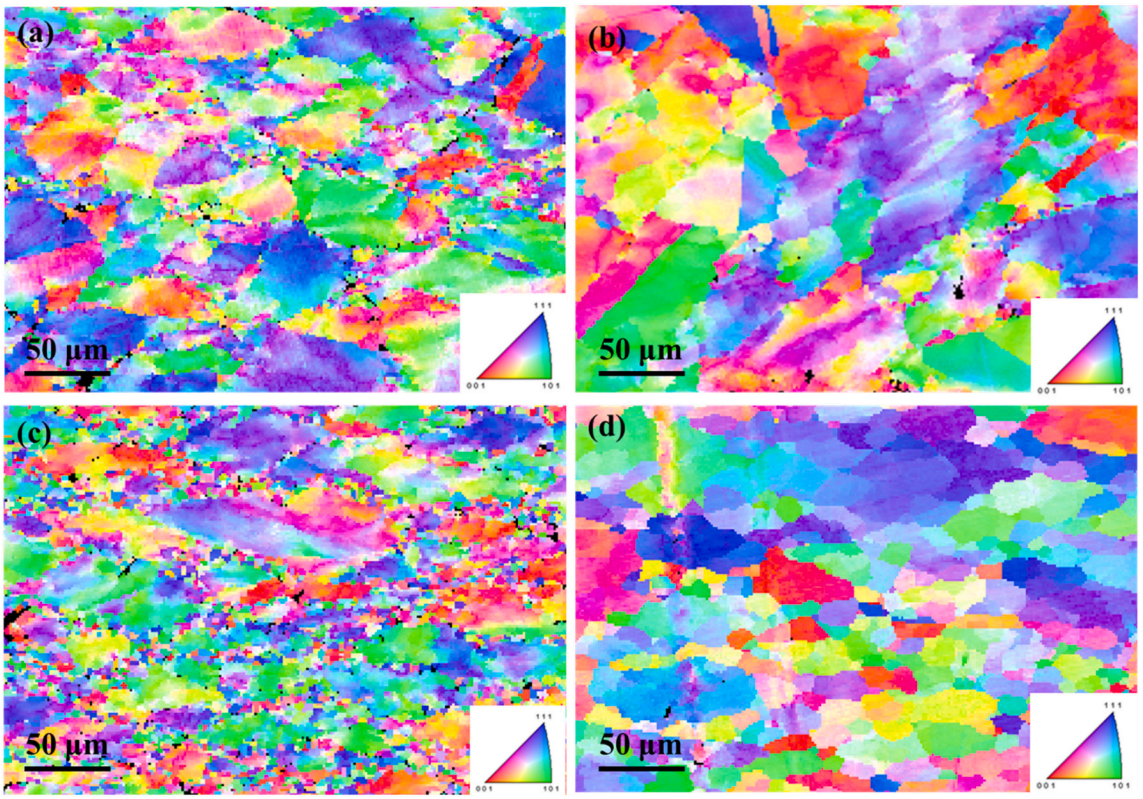

Fig. 3. EBSD images under different deformation conditions of Cu-2.6Co-0.65Si and Cu-2.6Co-0.65Si-0.2Y alloys deformed at 0.01 s^{-1} and different temperatures: (a) Cu-2.6Co-0.65Si alloy, 700 °C; (b) Cu-2.6Co-0.65Si, 900 °C; (c) Cu-2.6Co-0.65Si-0.2Y, 700 °C; (d) Cu-2.6Co-0.65Si-0.2Y, 900 °C.

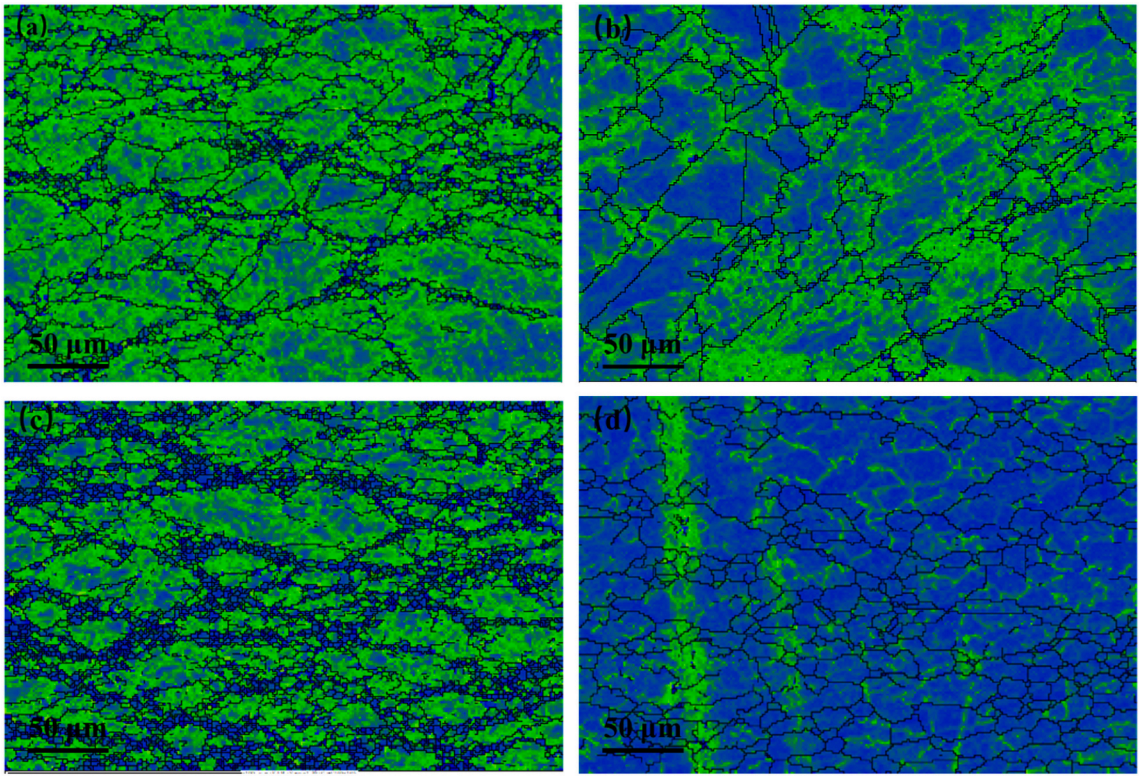

Fig. 4. EBSD orientation maps of Cu-2.6Co-0.65Si and Cu-2.6Co-0.65Si-0.2Y alloys deformed at 0.01 s^{-1} and different temperatures: (a) Cu-2.6Co-0.65Si alloy deformed at 700 °C, (b) Cu-2.6Co-0.65Si alloy deformed at 900 °C, (c) Cu-2.6Co-0.65Si-0.2Y alloy deformed at 700 °C, (d) Cu-2.6Co-0.65Si-0.2Y alloy deformed at 900 °C.

and consume the energy accumulated at grain boundaries by dislocations, so the number of small and medium angle grain boundaries in Fig. 4 (a) is significantly lower than Fig. 4 (b). Fig. 4 (c) and (d) are the orientation diagrams of alloy Cu-2.6Co-0.65Si and Cu-2.6Co-0.65Si-0.2Y at 700 °C and 900 °C, respectively. It can be clearly found that temperature increasing can promote dislocations movement and grain boundaries movement, and further reduce the number of low-angle boundary within the boundary. This also indicated that the nucleation and coarsening of DRX grains can consume the energy which was accumulated by dislocations, and consistent with the characteristics of DDRX [36].

In order to investigate the texture evolution of Cu-2.6Co-0.65Si and Cu-2.6Co-0.65Si-0.2Y alloys during hot deformation, the polar diagram and ODF maps of the two alloys were observed. The common recrystallization textures in copper alloys are the {011} ⟨100⟩ Goss texture, {112} ⟨111⟩ copper texture, {111} ⟨211⟩ R texture, {001} <100> cubic texture and {011} <211> brass texture [37,38]. When the temperature of the alloy increased from 700 °C to 900 °C, the main texture of the alloy changed from {001} <100> cubic texture to {011} <100> Goss texture. Compared with Fig. 5 (a) and (c), the maximum strength of the texture decreased from 23.635 to 6.073, which was indicated that the addition of rare earth Y reduced the texture strength of the Cu-2.6Co-0.65Si alloy.

3.4. TEM analysis

Fig. 6 shows the microstructure of Cu-2.6Co-0.65Si-0.2Y alloys at 700 °C and 0.001 s^{-1}. In the process of thermal deformation, a lot of dislocations were generated. Fig. 6 (a) shows that there were a lot of dispersed-distributed precipitates on the copper matrix. The movement of a single dislocation was hindered by multiple precipitates. Fig. 6 (b) shows the dislocation cells formed by the accumulation of each dislocation. The three-dimensional structure of dislocation aggregation in the cell wall forms a basically dislocation-free open area inside. Fig. 6 (c) shows the stacking faults caused by incomplete dislocations sweeping through the slip plane. Twins generated during thermal deformation are shown in Fig. 6 (d) and (e). The existence of twin boundaries can also hinder dislocation movement and delay dynamic recrystallization.

In the process of hot deformation, a large number of dislocations occurred, which will promote the precipitation and growth of solute atoms, and the interaction between the dislocations and the precipitated phase will hinder the movement of dislocations and improve the deformation resistance of the alloy in the process of hot deformation [39,40]. The interaction between dislocations and precipitates can be observed and analyzed to explain the change of flow stress and activation energy during hot deformation and inhibit the dynamic recrystallization process.

The Co and Ni elements have similar physical and chemical properties, and some related studies showed that the precipitated phase may be Co_2Si with similar structure to Ni_2Si [41]. Fig. 7 mainly shows the shape, size, type and crystal plane spacing of the precipitated phase. Fig. 7 (a) shows that the process of thermal deformation, the precipitated particles are nano particles, which are uniformly distributed on the copper matrix. Fig. 7 (b) is the SADP with a large precipitated phase of δ-Co_2Si and the lattice parameter in Co2Si is a = 0.0.710 nm, b = 0.491 nm, and c = 0.378 nm [42]. Fig. 7 (c) is HRTEM of the precipitated phase marked in (a), with a length of about 13.9 nm and a width of about 9.8 nm, and the measured result is 0.285 nm.

Fig. 8 shows TEM images of Cu-2.6Co-0.65Si alloy as control group at 700 °C. By comparing Fig. 6 (a) and Fig. 8 (b), it can be found that under the same magnification conditions, Cu-2.6Co-0.65Si-0.2Y alloy has smaller precipitated particles and more dislocations around the particles, which can greatly improve the flow stress of the alloy. The results show that the addition of Y promotes the precipitation of δ-Co_2Si and hinders the dislocation movement, thus improving the deformation resistance of the alloy during hot deformation. The reason for the Y

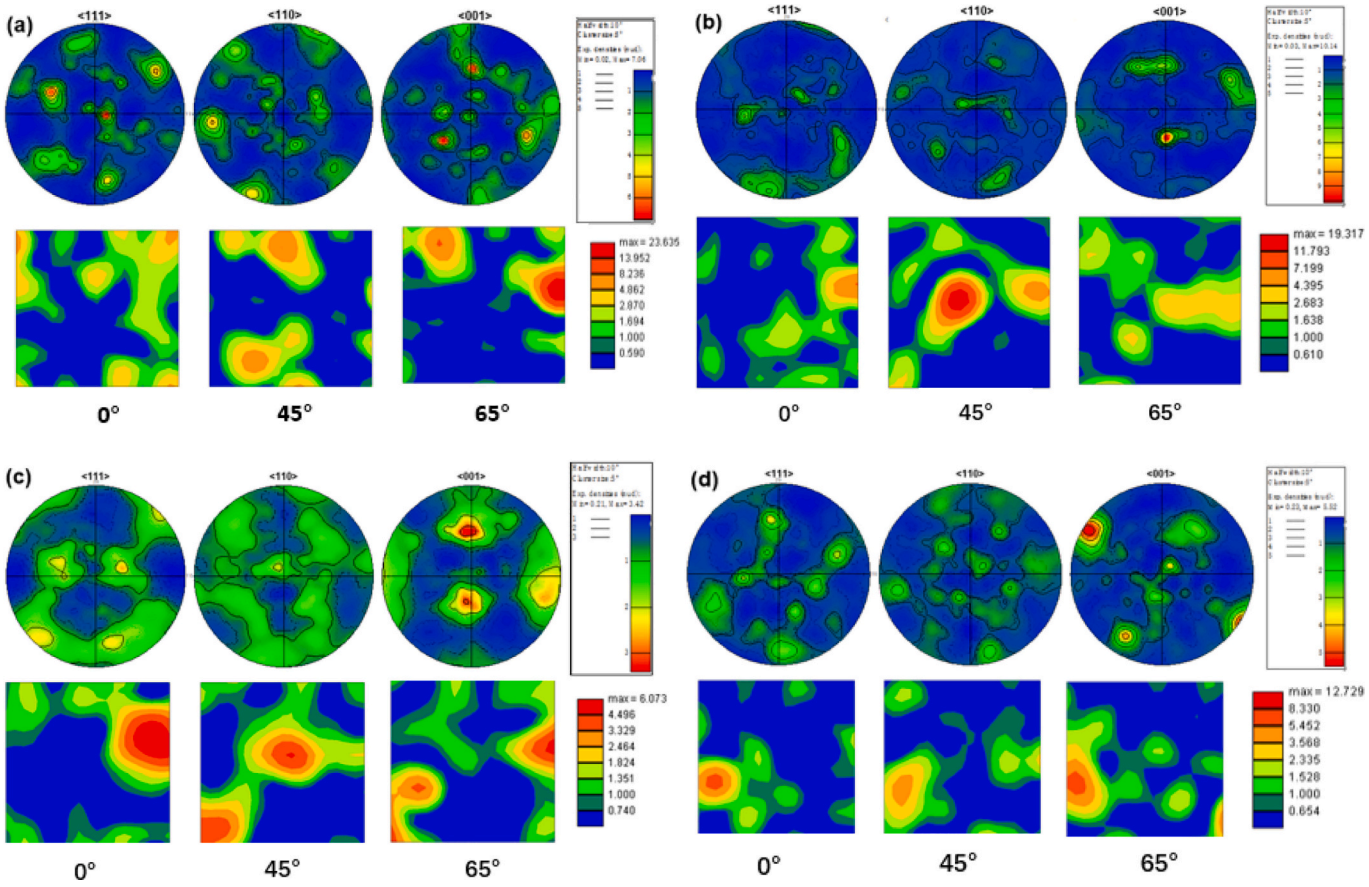

Fig. 5. DRXed-grains pole figure and DRXed-grains ODF maps of the Cu-2.6Co-0.65Si and Cu-2.6Co-0.65Si-0.2Y alloys: (a) Cu-2.6Co-0.65Si alloys deformed at 700 °C, (b) Cu-2.6Co-0.65Si alloys deformed at 900 °C, (c) Cu-2.6Co-0.65Si-0.2Y alloys deformed at 700 °C, (d) Cu-2.6Co-0.65Si-0.2Y alloys deformed at 900 °C.

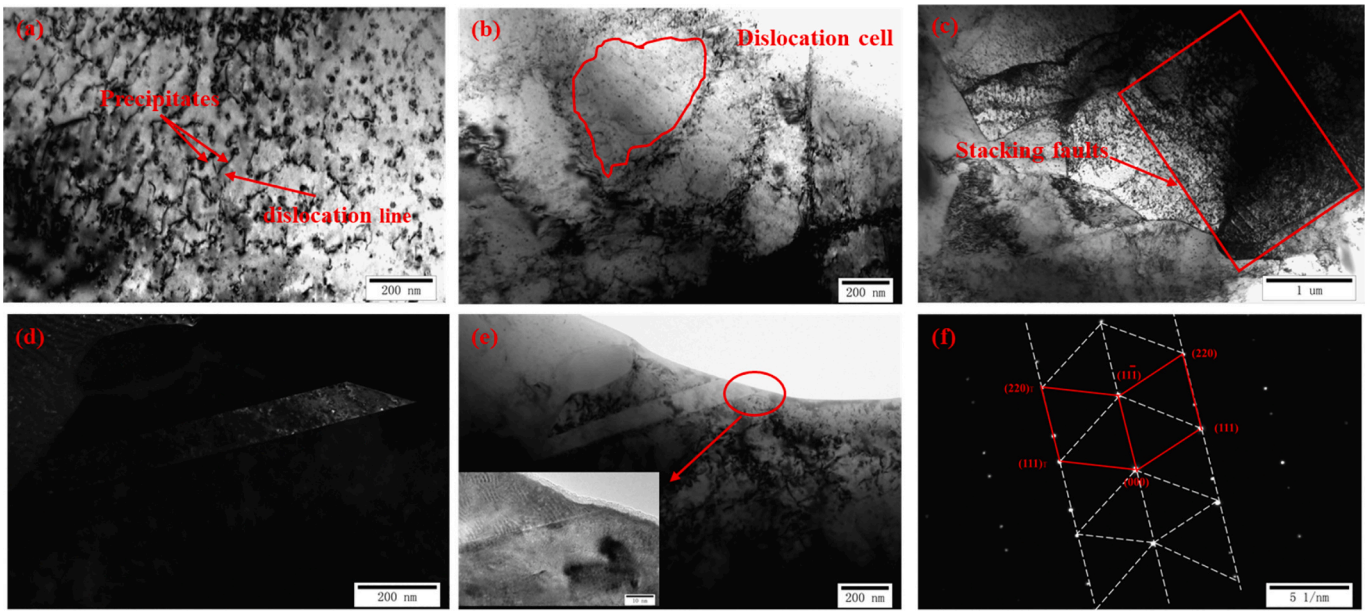

Fig. 6. TEM micrographs of Cu-2.6Co-0.65Si-0.2Y alloys deformed at 700 °C and 0.001 s^{-1}. (a) nanoscale precipitate and dislocation line, (b) dislocation cell, (c) stacking fault, (d) selected-area dark-field micrograph showing twin structure, (e) light field and twin plane, (d) SADP of twin.

addition can promote DRX and refine grain is that the Y addition can promote grain nucleation and inhibit grain growth. A large number of dislocations generated during hot deformation can provide favorable conditions for nucleation of DRX grains, resulting in a large number of fine grains. Dislocations can accelerate the movement of atoms in the metal and promote the precipitation of solute atoms. However, with the gradual strengthening of the inhibition effect of small precipitation relative to dislocation, the growth of DRX grain is inevitably inhibited,

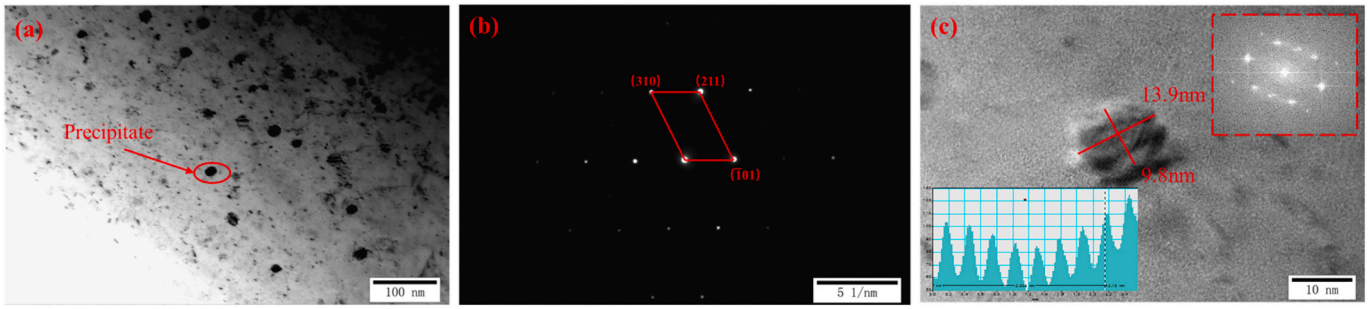

Fig. 7. TEM and HRTEM images of Cu-2.6Co-0.65Si-0.2Y alloys deformed at 700 °C and 0.001 s^{-1}. (a) the precipitates, (b) SADP corresponding to precipitate, (c) HRTEM images with the precipitate of (a).

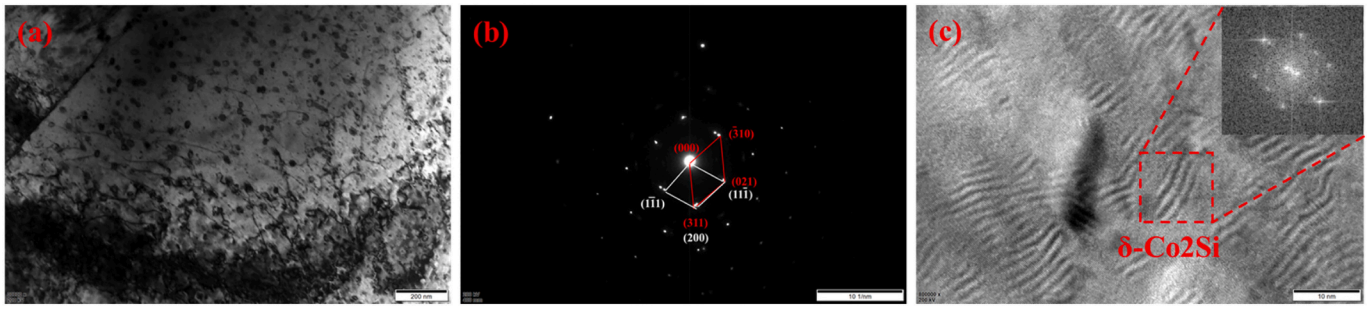

Fig. 8. TEM and HRTEM images of Cu-2.6Co-0.65Si alloys deformed at 700 °C and 0.001 s^{-1}. (a) the precipitates, (b) SADP corresponding of (a), (c) HRTEM images with the precipitate of (a).

and the DRX grain is refined.

According to the processing data obtained from hot deformation, it is found that Y can increase the flow stress of Cu-Co-Si alloy, that is, the deformation resistance during hot deformation is improved. In order to analyze the mechanism, EBSD and TEM were used to observe and analyze the microstructure evolution and precipitates of the two alloys, respectively. Through the analysis of EBSD data, it is found that Y promotes DRX behaviors in the process of hot deformation, and also improves the number of grains and large angle grain boundaries, which plays a positive role in improving the flow stress of the alloy. Through the further studies on the microstructure and precipitated phase of the alloy, it is found that Y can refine the precipitated phase and increase its quantity, which can hinder the dislocation migration, and improve the flow stress of the alloy.

4. Conclusions

The hot deformation behaviors of Cu-2.6Co-0.65Si and Cu-2.6Co-0.65Si-0.2Y alloys were investigated by Gleeble-1500 simulation deviced at strain rates of 0.001–10 s^{-1} and deformation temperatures of 500–900 °C. Through the compared analysis of the experimental results, the following conclusions can be drawn:

(1) Flow stress increased with strain rates and decreased with deformation temperatures, and dynamic recrystallization dominated the hot deformation process at high temperature.

(2) The hot deformation activation energies of Cu-2.6Co-0.65Si and Cu-2.6Co-0.65Si-0.2Y alloys were calculated to be 494.5 kJ·mol^{-1} and 533.6 kJ·mol-1, respectively. The constitutive equations of Cu-2.6Co-0.65Si and Cu-2.6Co-0.65Si-0.2Y alloys were deduced. The addition of a small amount of Y can increase the activation energy of hot deformation and the resistance of hot deformation of Cu-Co-Si alloy.

(3) The addition of Y promoted the nucleation of DRX grains and refined the recrystallized grains.

(4) A large number of dislocations and δ-Co_2Si particles are formed in the hot deformation process of Cu-Co-Si alloy, and the interaction between them impedes the dislocation migration and improves the deformation resistance of the alloy. In addition, the addition of Y promotes the precipitation of δ-Co_2Si.

Declaration of Competing Interest

The authors declared that they have no conflicts of interest to this work.

We declare that we do not have any commercial or associative interest that represents a conflict of interest in connection with the work.

Acknowledgments

This work was supported by the Outstanding Talents Innovation Fund of Henan Province (ZYQR201912164), Key Scientific Research Projects of Higher Education in Henan Province (21A430013), Natural Science Foundation of Henan Province (202300410144) and the National Natural Science Foundation of China (52071134).

References

[1] X.H. Zhang, Y. Zhang, B.H. Tian, K.X. Song, P. Liu, Y.L. Jia, X.H. Chen, J.C. An, Z. Zhao, Y. Liu, Review of Nano-Phase Effects in High Strength and Conductivity Copper Alloys, Nanotechnol, Rev., 2019, https://doi.org/10.1515/ntrev-2019-0034.

[2] H.Y. Yang, K.Q. Li, Y.Q. Bu, J.M. Wu, Y.T. Fang, L. Meng, J.B. Liu, H.T. Wang, Nanoprecipitates induced dislocation pinning and multiplication strategy for designing high strength, plasticity and conductivity Cu alloys, Scr. Mater. (2021), https://doi.org/10.1016/j.scriptamat.2021.113741.

[3] Z.L. Zhao, Z. Xiao, Z. Li, W.T. Qiu, H.Y. Jiang, Q. Lei, Z.R. Liu, Y.B. Microstructure and properties of a Cu–Ni–Si–Co–Cr alloy with high strength and high conductivity, Mater. Sci. Eng. (2019), https://doi.org/10.1016/j.msea.2019.05.003.

[4] X.H. Zhang, Y. Zhang, B.H. Tian, Y.L. Jia, Y. Liu, K.X. Song, Alex A. Volinsky, H. H. Xue, Cr effects on the electrical contact properties of the Al2O3-Cu/15W composites, Nanotechnol. Rev. (2019), https://doi.org/10.1515/ntrev-2019-0012.

[5] K.X. Song, Y.F. Geng, Y.J. Ban, Y. Zhang, Z. Li, X.J. Mi, J. Cao, Y.J. Zhou, X. B. Zhang, Effects of strain rates on dynamic deformation behavior of Cu-20Ag alloy, J. Mater. Sci. Technol (2021), https://doi.org/10.1016/j.jmst.2020.11.043.

[6] J.Z. Huang, Z. Xiao, J. Dai, Z. Li, H.Y. Jiang, W. Wang, X.X. Zhang, Microstructure and properties of a novel Cu-Ni-Co-Si-Mg alloy with super-high strength and

conductivity, Mat. Sci. Eng. A (2018), https://doi.org/10.1016/j.msea.2018.12.075.
[7] Z. Zhao, Y. Zhang, B.H. Tian, et al., Co effects on Cu-Ni-Si alloys microstructure and physical properties, J. Alloys Compd. (2019), https://doi.org/10.1016/j.jallcom.2019.05.135.
[8] X.P. Xiao, J. Huang, J.S. Chen, H. Xu, Z. Li, J.B. Zhang, Aging behavior and precipitation analysis of Cu-Ni-Co-Si Alloy, Crystals (2018), https://doi.org/10.3390/cryst8110435.
[9] J. Li, G.J. Huang, X.J. Mi, L.J. Peng, H.F. Xie, Y.L. Kang, Influence of the Ni/Co mass ratio on the microstructure and properties of quaternary Cu-Ni-Co-Si Alloys, Materials (2019), https://doi.org/10.3390/ma12182855.
[10] Y.J. Ban, Y. Zhang, Y.L. Jia, B.H. Tian, A.A. Volinsky, X.H. Zhang, Q.F. Zhang, Y. F. Geng, Y. Liu, Xu Li, Effects of Cr addition on the constitutive equation and precipitated phases of copper alloy during hot deformation, Mater. Design (2020), https://doi.org/10.1016/j.matdes.2020.108613.
[11] Y.F. Geng, X. Li, H.L. Zhou, Y. Zhang, Y.L. Jia, B.H. Tian, Y. Liu, A.A. Volinsky, X. H. Zhang, K.X. Song, G.X. Wang, L.H. Li, J.R. Hou, Effect of Ti addition on microstructure evolution and precipitation in Cu-Co-Si alloy during hot deformation, J. Alloys Compd. (2020), https://doi.org/10.1016/j.jallcom.2019.153518.
[12] Y.F. Geng, Y. Zhang, K.X. Song, Y.L. Jia, X. Li, H.R. Stock, H.L. Zhou, B.H. Tian, Y. Liu, A.A. Volinsky, X.H. Zhang, P. Liu, X.H. Chen, Effect of Ce addition on microstructure evolution and precipitation in Cu-Co-Si-Ti alloy during hot deformation, J. Alloys Compd. (2020), https://doi.org/10.1016/j.jallcom.2020.155666.
[13] K. Ma, Z.Y. Liu, X.X. Zhang, B.L. Xiao, Z.Y. Ma, Hot deformation behavior and microstructure evolution of carbon nanotube/7055Al composite, J. Alloys Compd. (2021), https://doi.org/10.1016/j.jallcom.2020.157275.
[14] J. Tang, J.H. Wang, J. Teng, G. Wang, D.F. Fu, H. Zhang, F.L. Jiang, Effect of Zn content on the dynamic softening of Al–Zn–Mg–Cu alloys during hot compression deformation, Vacuum (2021), https://doi.org/10.1016/j.vacuum.2020.109941.
[15] X. Wang, Z. Li, Z. Xiao, W.T. Qiu, Microstructure evolution and hot deformation behavior of Cu−3Ti−0.1Zr alloy with ultra-high strength, T. Nonferr. Metal. Soc (2020), https://doi.org/10.1016/S1003-6326(20)65416-4.
[16] J.C. Long, Q.X. Xia, G.F. Xiao, Y. Qin, S. Yuan, Flow characterization of magnesium alloy ZK61 during hot deformation with improved constitutive equations and using activation energy maps, Int. J. Mech. Sci. (2021), https://doi.org/10.1016/j.ijmecsci.2020.106069.
[17] P.H. Geng, G.L. Qin, J. Zhou, T.Y. Li, N.S. Ma, Characterization of microstructures and hot-compressive behavior of GH4169 superalloy by kinetics analysis and simulation, J. Mater. Process. Technol. (2021), https://doi.org/10.1016/j.jmatprotec.2020.116879.
[18] Y.F. Xia, W. Jiang, Q. Cheng, Hot deformation behavior of Ti−6Al−4V−0.1Ru alloy during isothermal compression, T. Nonferr Metal. Soc (2020), https://doi.org/10.1016/S1003-6326(19)65186-1.
[19] K. Arun Babu, S. Mandal, C.N. Athreya, B. Shakthipriya, V. Subramanya Sarma, Hot deformation characteristics and processing map of a phosphorous modified super austenitic stainless steel, Mater. Design (2017), https://doi.org/10.1016/j.matdes.2016.11.054.
[20] W.Y. Wang, J.L. Zhu, N.N. Qin, Y.F. Zhang, S.Y. Li, Z. Xiao, Q. Lei, Z. Li, Effects of minor rare earths on the microstructure and properties of Cu-Cr-Zr alloy, J. Alloys Compd. (2020), https://doi.org/10.1016/j.jallcom.2020.155762.
[21] Y. Zhan, H.L. Sun, A.A. Volinsky, B.J. Wang, B.H. Tian, Z. Chai, Y. Liu, K.X. Song, Small Y addition effects on hot deformation behavior of copper-matrix alloys, Adv. Eng. Mater. (2017), https://doi.org/10.1002/adem.201700197.
[22] B.J. Wang, Y. Zhang, B.H. Tian, J.C. An, A.A. Volinsky, H.L. Sun, Y. Liu, K.X. Song, Effects of Ce addition on the Cu-Mg-Fe alloy hot deformation behavior, Vacuum (2018), https://doi.org/10.1016/j.vacuum.2018.06.006.
[23] Y. Zhang, H.L. Sun, A.A. Volinsky, B.J. Wang, B.H. Tian, Y. Liu, K.X. Song, Constitutive model for hot deformation of the Cu-Zr-Ce alloy, J. Mater. Eng. Perform. (2018), https://doi.org/10.1007/s11665-018-3168-2.
[24] B.J. Wang, Y. Zhang, B.H. Tian, Vladislav Yakubov, J.C. An, Alex A. Volinsky, Y. Liu, K.X. Song, L.H. Li, M. Fu, Effects of Ce and Y addition on microstructure evolution and precipitation of Cu-Mg alloy hot deformation, J. Alloys Compd. (2019), https://doi.org/10.1016/j.jallcom.2018.12.022.
[25] L.X. Wang, G. Fang, M.A. Leeflang, J. Duszczyk, J. Zhou, Constitutive behavior and microstructure evolution of the as-extruded AE21 magnesium alloy during hot compression testing, J. Alloys Compd. (2015), https://doi.org/10.1016/j.jallcom.2014.10.006.
[26] F. Liu, J.M. Ma, L.J. Peng, G.J. Huang, W.J. Zhang, H.F. Xie, X.J. Mi, Hot Deformation Behavior and Microstructure Evolution of Cu–Ni–Co–Si Alloys, Materials (2020), https://doi.org/10.3390/ma13092042.
[27] C.M. Sellars, W.J. McTegart, On the mechanism of hot deformation, Acta Metall. 14 (1966) 1136–1138.
[28] C. Zener, J.H. Hollomon, Effect of strain-rate upon the plastic flow of steel, J. Appl. Phys. 15 (1994) 22–27.
[29] Y.F. Geng, Y.J. Ban, B.J. Wang, X. Li, K.X. Song, Y. Zhang, Y.L. Jia, B.H. Tian, Y. Liu, A.A. Volinsky, A review of microstructure and texture evolution with nanoscale precipitates for copper alloys, J. Mater. Res. Technol (2020), https://doi.org/10.1016/j.jmrt.2020.08.055.
[30] R. Mishnev, I. Shakhova, A. Belyakov, R. Kaibyshev, Deformation microstructures, strengthening mechanisms, and electrical conductivity in a Cu-Cr-Zr alloy, Mater. Sci. Eng. A (2015), https://doi.org/10.1016/j.msea.2015.01.065.
[31] F. Bittner, S. Yin, A. Kauffmann, J. Freudenberger, H. Klauß, G. Korpala, R. Kawalla, W. Schillinger, L. Schultz, Dynamic recrystallisation and precipitation behavior of high strength and highly conducting Cu-Ag-Zr alloys, Mater. Sci. Eng. (2014), https://doi.org/10.1016/j.msea.2013.12.051.
[32] C. Zhao, Z. Wang, D.Q. Pan, D.X. Li, Z.Q. Luo, D.T. Zhang, C. Yang, W.W. Zhang, Effect of Si and Ti on dynamic recrystallization of high-performance Cu−15Ni−8Sn alloy during hot deformation, T. Nonferr. Metal. Soc (2019), https://doi.org/10.1016/S1003-6326(19)65163-0.
[33] J.Y. Yang, W.J. Kim, The effect of addition of Sn to copper on hot compressive deformation mechanisms, microstructural evolution and processing maps, J. Mater. Res. Technol (2020), https://doi.org/10.1016/j.jmrt.2019.11.015.
[34] J. Liu, X.H. Wang, J.T. Liu, Y.F. Liu, H.Y. Li, C. Wang, Hot deformation and dynamic recrystallization behavior of Cu-3Ti-3Ni-0.5Si alloy, J. Alloys Compd. (2019), https://doi.org/10.1016/j.jallcom.2018.12.212.
[35] K. Huang, K. Marthinsen, Q.L. Zhao, R.E. Loge, The double-edge effect of second-phase particles on the recrystallization behaviour and associated mechanical properties of metallic materials, Prog. Mater. Sci. (2017), https://doi.org/10.1016/j.pmatsci.2017.10.004.
[36] Y.J. Ban, Y. Zhang, B.H. Tian, K.X. Song, M. Zhou, X.H. Zhang, Y.L. Jia, X. Li, Y. Liu, A.A. Volinsky, EBSD analysis of hot deformation behavior of Cu-Ni-Co-Si-Cr alloy, Mater. Charact. (2020), https://doi.org/10.1016/j.matchar.2020.110656.
[37] C.S. Wang, H.D. Fu, J.X. Xie, Dynamic recrystallization behavior and microstructure evolution of high-performance Cu-3.28Ni-0.6Si-0.22Zn-0.11Cr-0.04P during hot compression, Rare Metals (2021), https://doi.org/10.1007/s12598-020-01578-z.
[38] C. Haase, L.A. Barrales-Mora, Influence of deformation and annealing twinning on the microstructure and texture evolution of face-centered cubic highentropy alloys, Acta Mater. (2018), https://doi.org/10.1016/j.actamat.2018.02.048.
[39] M.Y. Li, H. Wang, Y.H. Guo, H.L. Wang, D.D. Zheng, J.F. Shan, Y.Q. Chang, Microstructures and mechanical properties of the novel CuCrZrFeTiY alloy for fusion reactor, J. Nucl. Mater. (2020), https://doi.org/10.1016/j.jnucmat.2020.152063.
[40] J. Yi, Y.L. Jia, Y.Y. Zhao, Z. Xiao, K.J. He, Q. Wang, M.P. Wang, Z. Li, Precipitation behavior of Cu-3.0Ni-0.72Si alloy, Acta Mater. (2018), https://doi.org/10.1016/j.actamat.2018.12.047.
[41] S. Geller, V.M. Wolontis, The crystal structure of Co_2Si, Acta Crystallogr. 8 (2) (1955) 83–87.